



## OPEN

SUBJECT AREAS:  
CARBON NANOTUBES  
AND FULLERENES  
BATTERIESReceived  
4 October 2013Accepted  
18 December 2013Published  
16 January 2014Correspondence and  
requests for materials  
should be addressed to  
B.W. (edward.  
bwang@gmail.com) or  
J.L.C. (jenny.jlcheng@  
gmail.com)

# Mesoporous CNT@TiO<sub>2</sub>-C Nanocable with Extremely Durable High Rate Capability for Lithium-Ion Battery Anodes

Bin Wang<sup>1,2</sup>, Huolin Xin<sup>3</sup>, Xiaodong Li<sup>1,2</sup>, Jianli Cheng<sup>1,2</sup>, Guangcheng Yang<sup>1</sup> & Fude Nie<sup>1</sup><sup>1</sup>Institute of Chemical Materials, China Academy of Engineering Physics, P.O.BOX 919–328 Mianyang, Sichuan 621900, China, <sup>2</sup>Sichuan research center of new materials, Chengdu, Sichuan 610207, China, <sup>3</sup>Materials Science Division, Lawrence Berkeley National Laboratory, Berkeley, CA, 94720, USA.

A well-designed nanostructure CNT@TiO<sub>2</sub>-C with fine anatase TiO<sub>2</sub> particle (< 8 nm), good electronic conducting network (inner CNT core and outer carbon layer), and mesoporous structure was prepared by a simple and green one-pot hydrothermal reaction. The utilization of glucose in the hydrothermal process not only solves the interfacial incompatibility between CNTs and titanate sol and controls the nucleation and growth of TiO<sub>2</sub> particles, but also introduces a uniform, glucose-derived, carbon-layer on the TiO<sub>2</sub> particles. The nanosized TiO<sub>2</sub> particle, high conducting network, and interconnected nanopores of the CNT@TiO<sub>2</sub>-C nanocable greatly improve its electrochemical performances, especially rate capability. The CNT@TiO<sub>2</sub>-C nanocables show remarkable rate capability with reversible charge capacity of 297, 240, 210, 178 and 127 mAh g<sup>-1</sup> at 1C, 5C, 10C, 20C and 50C, respectively, as well as excellent high rate cycling stability with capacity retention of 87% after 2000 cycles at 50C.

TiO<sub>2</sub> has attracted much attention because of its superior chemical and physical properties, and potential applications in gas sensing<sup>1</sup>, photocatalysis<sup>2</sup>, and lithium-ion batteries (LIBs)<sup>3,4</sup>. TiO<sub>2</sub> with different polymorphs (anatase, rutile, and bronze) has been extensively studied as an alternative to the carbonaceous anode for LIBs. Anatase TiO<sub>2</sub> as an anode material has generated special interests owing to its high electrochemical activity, low toxicity, chemical stability, low price, and safety. Its high lithium ion insertion/extraction potential at ~1.7 V (versus Li<sup>+</sup>/Li) is inherently safe because of avoiding the Li-dendrite electroplating. Furthermore, the limited volume change (less than 4%) during the Li<sup>+</sup> insertion/extraction process leads to an enhanced structural stability and a prolonged cycling life<sup>5</sup>. However, the poor ionic and electronic conductivity of anatase TiO<sub>2</sub> and the limited specific capacity (Li<sub>x</sub>TiO<sub>2</sub> (x ≤ 0.5), x = 0.5, 168 mAh/g) pose challenges to meet the requirements for high-power-density and high-energy-density LIBs.

To address this issue, many kinds of nanostructures with different morphologies and different hierarchical structures have been investigated<sup>4,6</sup>. Tailoring the particle size of TiO<sub>2</sub> and constructing porous channel in the material are employed to improve the practical capacity and the rate capability of TiO<sub>2</sub> anode. The nanosized particles with large specific surface area decrease the current density per unit surface area and shorten the Li<sup>+</sup>-diffusion length in the solid phase, thus enabling Li<sup>+</sup> to transport rapidly into the interior of TiO<sub>2</sub>. Meanwhile, the significant increase of the surface and the interface area in nanosized materials can improve the capacity beyond that of conventional bulk materials<sup>7–9</sup>. Enhancing the electrochemical performances—high specific capacity (Li<sub>x</sub>TiO<sub>2</sub> (x > 0.5)) and high-rate capability—are thus obtained accordingly using porous and nanometer-sized TiO<sub>2</sub> electrode<sup>10–13</sup>. Another way to improve the electronic conductivity of TiO<sub>2</sub> is to connect nanostructured TiO<sub>2</sub> materials with highly conductive materials to yield a hybrid nanostructure. High rate capability has been reported for nanostructured networks of TiO<sub>2</sub>-RuO<sub>2</sub> composites<sup>13</sup>, TiO<sub>2</sub>-carbon nanotube(CNT) hybrid structures<sup>10,14</sup>, TiO<sub>2</sub>-ITO(indium tin oxide) nanocomposites<sup>15</sup>, TiO<sub>2</sub>-graphene hybrid structures<sup>16,17</sup>, and carbon-coating TiO<sub>2</sub> composites<sup>18,19</sup>. Among various conductive materials, the one-dimensional CNT with high electronic conductivity, high mechanical strength, and large-scale availability is an ideal conducting substrate; thus it is widely investigated in the field of energy conversion and storage<sup>10,20–23</sup>. However, pristine CNTs synthesized by chemical vapor deposition are hydrophobic. As a result, it is difficult for TiO<sub>2</sub> to directly nucleate and grow on the surface of pristine CNTs<sup>24–26</sup>. Therefore, two main challenges are posed for synthesizing hybrid CNT-TiO<sub>2</sub> materials for high-performance anodes of LIBs. The first issue is how to improve the interfacial interaction between TiO<sub>2</sub> and CNTs. And another issue is how to control TiO<sub>2</sub> particle size while introducing a porous



surface. It was previously reported that hydroxyl and carboxyl groups on the surface of CNT introduced by strong acid oxidation could provide covalent-bonding interfacial interaction between the titanate sol and CNTs<sup>27,28</sup>. However, the acid oxidation treatments also inevitably shorten the CNT and destroy the structure of CNT which degrade its electronic conductivity and mechanical strength. Recently, Eder *et al.*<sup>24,25</sup> reported a non-covalent process to enable coating of TiO<sub>2</sub> on the CNTs by using benzyl alcohol (BA) as the surfactant. The phenyl ring of the BA attached to the graphitic surface of CNTs *via*  $\pi$ - $\pi$  stacking, and then the hydroxyl group of the BA interacted directly with the precursors in the sol-gel process as linkers<sup>29</sup>. Hence, BA enables the synthesis of CNT-inorganic hybrid materials without the requirement of covalent functionalization of CNT. However, the uses of extra additives undoubtedly increase the synthesis complexity, the cost, and pose potential hazards to the environment. Therefore, it is highly desirable but quite challenging to design a simple and green route to integrate TiO<sub>2</sub> with highly conductive CNTs at nanoscale for using as high-performance anode material.

In this work, we present a simple and green one-pot route to form a new nanostructured CNT@TiO<sub>2</sub>-C nanocable by using glucose as structure-directing agent and carbon source without any prerequisite for covalent/non-covalent functionalization of CNTs. Although glucose is often used as a carbon source in hydrothermal reactions<sup>30–32</sup>, it is the first time to be used as a structure-directing agent to form CNT@TiO<sub>2</sub>-C nanocable. It was reported that some aromatic compounds can be produced during the hydrothermal process of glucose<sup>31,33</sup>. Therefore, it can be expected that these aromatic compounds with multiple hydroxyl groups originated from glucose can act as a bridge to connect TiO<sub>2</sub> and CNTs by  $\pi$ - $\pi$  interactions just like the BA surfactant<sup>24,25</sup>. Consistent with the hypothesis, using the glucose as structure-directing agent and carbon source, a new hybrid nanostructure CNT@TiO<sub>2</sub>-C nanocable with high electronic and ionic conducting network was prepared in one pot, which showed high specific capacity, superior rate capability, and excellent long-term cycling stability as anode material for LIBs in half cell. Figure 1 shows the one-pot hydrothermal routine to prepare the CNT@TiO<sub>2</sub>-C nanocable. Using glucose to facilitate the formation of CNT@TiO<sub>2</sub>-C nanocable in one pot presents multiple highlights: 1) the utilization of glucose not only solves the interfacial incompatibility between CNTs and titanate sol, but also provides molecular template to control the nucleation and growth of TiO<sub>2</sub>; 2) the carbon-rich polysaccharide derived from the glucose can integrate the TiO<sub>2</sub> nanoparticles with high electronic conductive CNT core to form a three-dimensional electronic conducting network; 3) the whole process is simple and intrinsically green because it only uses CNTs, titanium isopropoxide, and glucose as the precursors (see Experimental Section for more details); 4) glucose is an abundant and environmentally benign product, which can reduce the cost of the hybrid material.

## Results

The morphology of the prepared CNT@TiO<sub>2</sub>-C hybrid material was characterized by scanning electron microscopy (SEM), high resolution transmission electron microscopy (HR-TEM), and Z-contrast annular dark-field scanning transmission electron microscopy (ADF-STEM). Compared with pristine CNTs shown in Fig. 2a, the CNT@TiO<sub>2</sub>-C nanocables preserve the one-dimensional nanostructure of the CNT with the diameters ranging from 20 to 30 nm (Fig. 2b–c). The surfaces of CNTs become coarse, indicating the coating of TiO<sub>2</sub> and carbon. The transmission electron microscopy (TEM) images in Fig. 2d show that a thin carbon layer was continuously wrapped on the TiO<sub>2</sub> nanoparticles. The presence of the carbon layer resulted from the carbonization of glucose derivatives can effectively improve the electronic conductivity of the hybrid material. Meanwhile, the carbon layer can act as a separator to restrain the

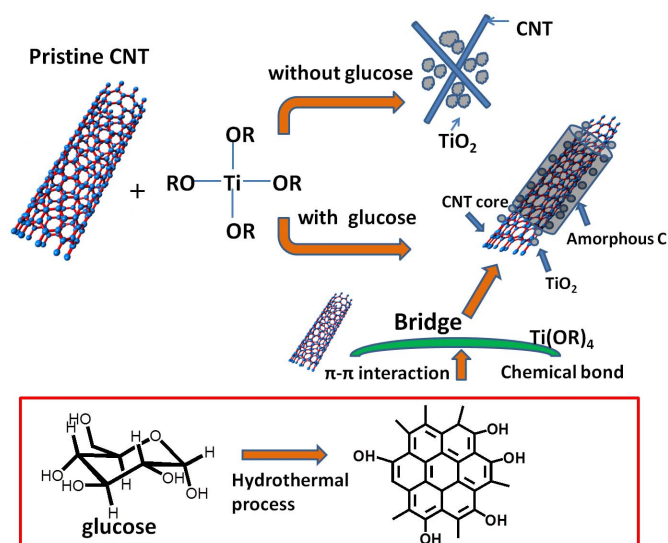


**Figure 1** | Schematic illustration of the one-pot hydrothermal routine to prepare CNT@TiO<sub>2</sub>-C nanocable with the assistance of glucose.

growth of primary TiO<sub>2</sub> nanoparticles during the hydrothermal and annealing process and therefore keep the particle size at nanoscale. The crystallite sizes are below 8 nm as determined from TEM images. The lattice fringes observed in HR-TEM image (Fig. 2e) and its corresponding fast Fourier transform (FFT) pattern in Fig. 2f reveal the crystal structure to be anatase TiO<sub>2</sub>. From ADF-STEM Z-contrast images (Fig. 2g), it is shown that the high-contrast TiO<sub>2</sub> nanoparticles covering on the surface of CNT are relatively homogeneous. The near-edge fine structure of the Ti L<sub>2,3</sub> edge in the electron energy loss spectrum designates the nanoparticles to be stoichiometric TiO<sub>2</sub>. To better illustrate the nanostructure of the CNT@TiO<sub>2</sub>-C, more SEM and TEM images at different magnifications are provided in supplementary Fig. S1 and Fig. S2. Nitrogen isothermal adsorption-desorption measurements were performed to determine the Brunauer-Emmett-Teller (BET) surface area and the porosity of the prepared material. Supplementary Fig. S3 shows the adsorption/desorption isotherms of CNT@TiO<sub>2</sub>-C nanocables, which exhibits a hysteresis of typical type IV isotherm, demonstrating a porous structure with a BET specific surface area of 75.8 m<sup>2</sup> g<sup>-1</sup>.

The XRD pattern of the CNT@TiO<sub>2</sub>-C nanocable is shown in Fig. 3a. The diffraction pattern is in good agreement with anatase TiO<sub>2</sub> (JCPDS 21-1272). Raman spectra were carried out to investigate the crystalline phase of TiO<sub>2</sub> and the carbon type in the nanocable (Fig. 3b). Four peaks with strong intensities at 146, 395, 515, and 635 cm<sup>-1</sup> can be observed in the Raman spectra of the CNT@TiO<sub>2</sub>-C nanocable, which are well consistent with that of reported anatase TiO<sub>2</sub><sup>14</sup>. Furthermore, two characteristic peaks located at about 1372 and 1592 cm<sup>-1</sup> correspond to disorder carbon (D-band) and graphite carbon (G-band) in the nanocable, respectively. The peak intensity ratio of D-band and G-band ( $I_D/I_G$ ) is found to be 1.5 for CNT@TiO<sub>2</sub>-C nanocable compared with the  $I_D/I_G$  value of pristine CNTs (about 1.0), which clearly demonstrates the existence of amorphous carbon in CNT@TiO<sub>2</sub>-C nanocable. The total carbon content including carbon nanotube and amorphous carbon is directly obtained from the TGA (see supplementary Fig. S4 online).

To unravel the impact of the glucose and CNTs on the structure formation, the samples were prepared in the absence of glucose and CNTs. In sharp contrast, in the absence of the glucose, TiO<sub>2</sub> precipitated in form of large clusters (named as CNT/TiO<sub>2</sub> composite) without the formation of the nanocable (Fig. 4a–b). Without the addition of CNT and glucose, only agglomerated TiO<sub>2</sub> nanoparticles were obtained (Fig. 4c–d). Eder *et al.*<sup>24,25</sup> reported that the surface properties of CNTs were crucial to control the morphology and



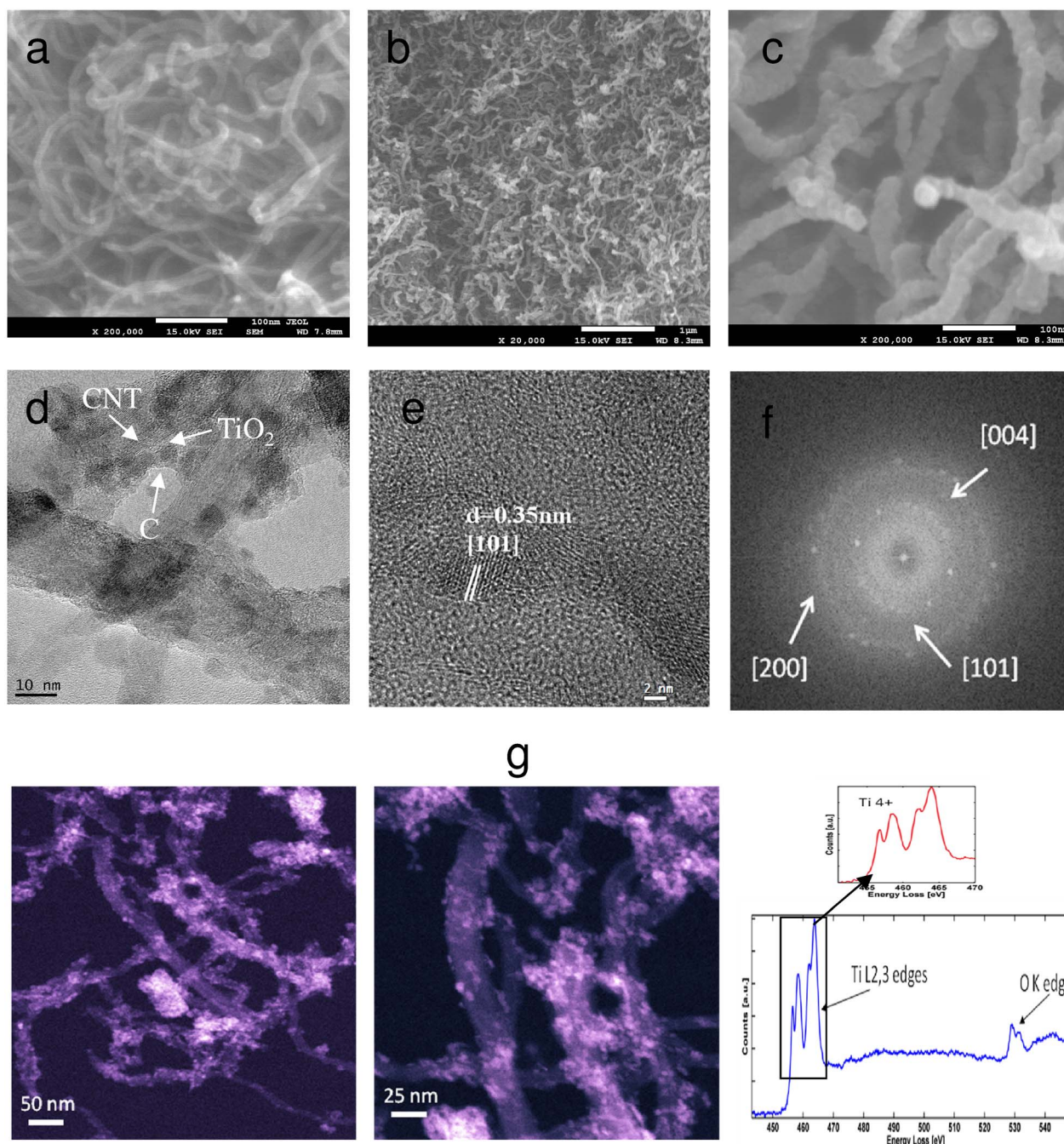


**Figure 2 | Morphology and structure.** SEM images of (a) pristine CNT and (b,c) CNT@TiO<sub>2</sub>-C nanocable; (d) TEM image and (e) HR-TEM image of CNT@TiO<sub>2</sub>-C nanocable; (f) Fast Fourier transform pattern of (e); (g) Annular dark-field scanning transmission electron microscopy (ADF-STEM) Z-contrast image of CNT@TiO<sub>2</sub>-C nanocable and electron energy loss spectrum of the TiO<sub>2</sub> supported on the CNT.

structure of the TiO<sub>2</sub> coating. Therefore, we speculate that the glucose alters the surface property of CNT and plays a role as a structure-directing agent in the formation of the CNT@TiO<sub>2</sub>-C nanocables. It has been reported that the dehydration and aromatization usually occur during the hydrothermal reaction of glucose<sup>31,33–35</sup>. The FT-IR spectrum was used to track the process (see supplementary Fig. S5 online). The increase in the intensity of the band at 1620 cm<sup>−1</sup> (C=C) for CNT@TiO<sub>2</sub>-C nanocables in comparison with pristine CNT and CNT/TiO<sub>2</sub> composite supports the aromatization of glucose during the hydrothermal process. Meanwhile, the appearance of the bands in the range of 1000–1300 cm<sup>−1</sup>, which can be assigned to the C-OH stretching and O-H bending vibrations, implies the existence of large quantities of hydroxyl groups. In

accordance with our speculation, these aromatic compounds with a lot of hydroxyl groups resulted from the glucose aromatization act as the bridge to connect TiO<sub>2</sub> and CNT by  $\pi$ - $\pi$  interactions. Apart from being a structure-directing agent, the glucose also affects the crystallization and grain growth of TiO<sub>2</sub> crystal. The effect of glucose on crystal was clarified by XRD, which shows that the diffraction peaks become broader with the increasing of the glucose content (see supplementary Fig. S6 online). Even annealed at 700°C for 3 h, most of the diffraction peaks of the product synthesized by adding the higher content of glucose are still too broad to be detected. According to the Scherrer formula, it demonstrates that the average crystallite size in CNT@TiO<sub>2</sub>-C nanocable decreases with increasing the amount of glucose in the hydrothermal reaction. Presumably, the

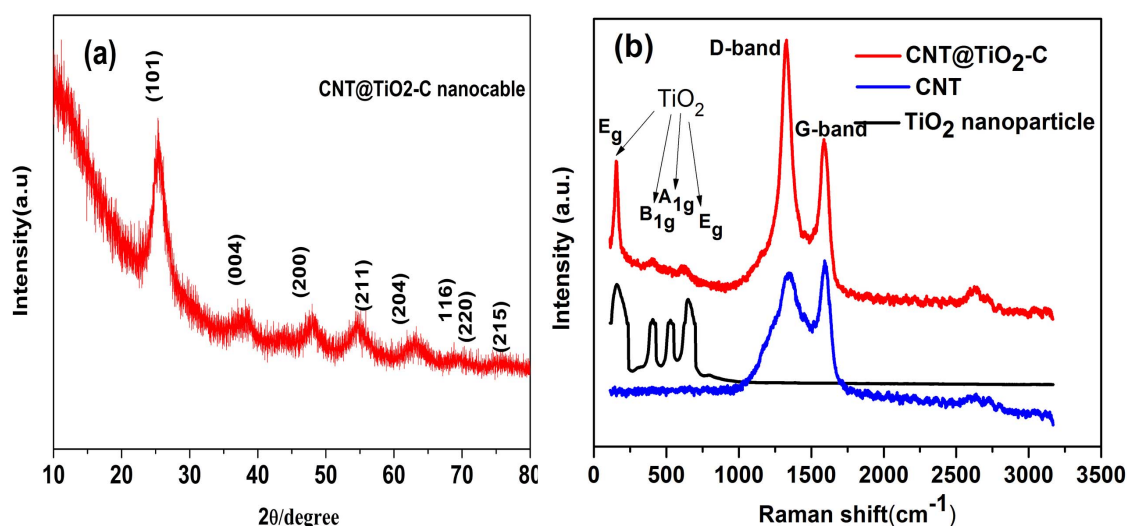


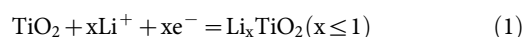
**Figure 3** | (a) XRD pattern of CNT@TiO<sub>2</sub>-C nanocable; (b) Raman spectra of CNT@TiO<sub>2</sub>-C nanocable, TiO<sub>2</sub> nanoparticle, and pristine CNT.

glucose-derived compounds absorbing on titania nanoparticle limited further structural growth and the final size of TiO<sub>2</sub>, which is similar to the surfactant<sup>24</sup>. Therefore, it can be concluded that the glucose plays multi-roles in the formation of the CNT@TiO<sub>2</sub>-C nanocable, including structure-directing agent, carbon source, and surfactant.

## Discussion

To understand the electrochemical behavior of this hybrid material, we investigated the performance of the CNT@TiO<sub>2</sub>-C nanocable as an anode material of LIBs. Figure 5a shows the cyclic voltammograms (CV) of the CNT@TiO<sub>2</sub>-C nanocable electrode for the first five scans at a scan rate of 0.1 mV s<sup>-1</sup>. Two peaks at approximately 1.73 V (cathodic) and 1.98 V (anodic) are associated with Li<sup>+</sup> insertion/extraction into/from the anatase. It is worth noting that the CV curve shows an ideal rectangular shape in the range of 1.0–1.7 V, which is characteristic of charging/discharging of supercapacitance contributed from the TiO<sub>2</sub> and carbon. Furthermore, these peaks show almost no change in amplitude and voltage positions during

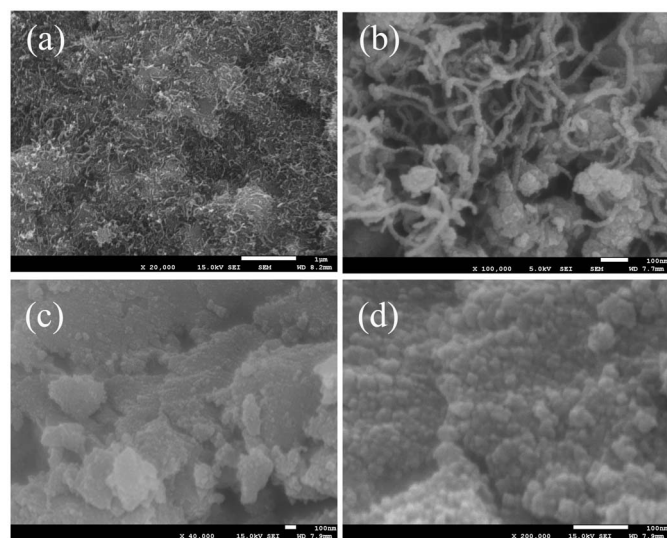
the subsequent several cycles, indicating good stability and high reversibility of the electrochemical reaction presented in equation (1).



Where,  $x$  is the amount of inserted Li<sup>+</sup> in anatase and it depends upon the crystallite size and nanostructure of the TiO<sub>2</sub> materials<sup>8,9,36</sup>.

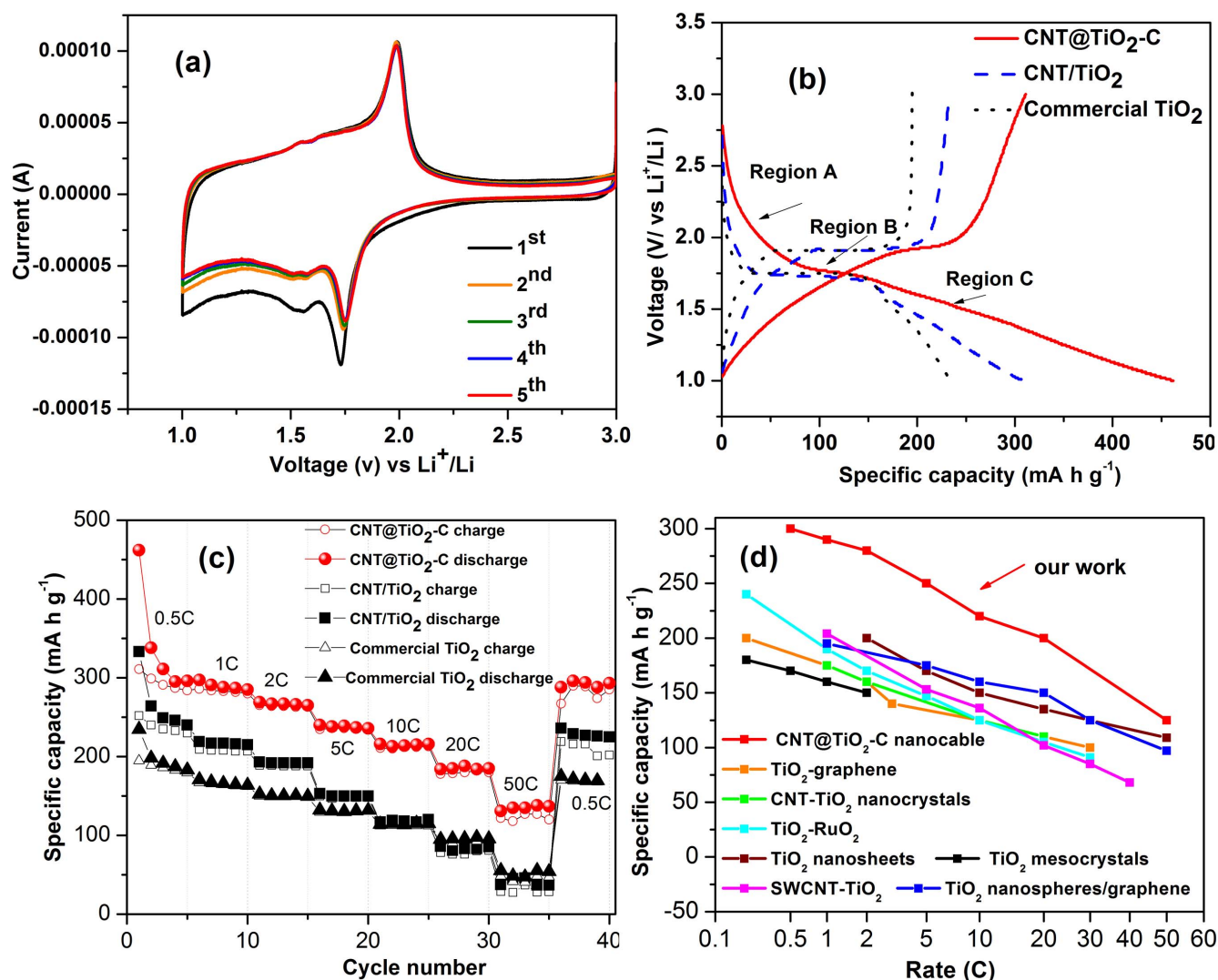
To better know the electrochemical performance of the CNT@TiO<sub>2</sub>-C nanocable, CNT/TiO<sub>2</sub> composite synthesized in the absence of glucose and commercial TiO<sub>2</sub> (particle size <25 nm) were studied as counterparts. Figure 5b shows the charge-discharge profiles of the CNT@TiO<sub>2</sub>-C nanocable, CNT/TiO<sub>2</sub> composite, and commercial TiO<sub>2</sub> at a rate of 0.5 C. The voltage profiles of the three TiO<sub>2</sub> materials in the first discharge process show three distinct regions. Region A ranging from OCV to ~1.75 V shows a rapid voltage drop, which is known as a homogeneous Li<sup>+</sup> insertion into the bulk by a solid-solution insertion mechanism<sup>7</sup>. A well-known two-phase plateau in region B is observed at ~1.75 V, where Li-rich phases and Li-poor phases coexist<sup>5</sup>. After the two-phase plateau, the region C at below 1.75 V exhibits a sloped curve. This process can be attributed to the reversible surface/interfacial lithium storage on the TiO<sub>2</sub> and carbon, which is consistent with the above rectangular curves in the CV shown in Fig 5a. Supplementary Table S1 summarizes the capacities corresponding to the three different electrochemical processes in the first cycle. It can be observed that the region A and B provide a large proportion of lithium storage contribution for the commercial TiO<sub>2</sub> nanoparticle, which has the largest region B and relatively smaller region C. The CNT/TiO<sub>2</sub> composite has a relatively long region B as well as a long region C. In sharp contrast, the CNT@TiO<sub>2</sub>-C nanocable has a very small region B and the largest region C as the main lithium storage region. It is consistent with the reported results that the proportion of region A+B decreases, while region C increases with a decreasing of the TiO<sub>2</sub> particle size<sup>8,37</sup>. It should be mentioned that these sloped charge-discharge voltage profiles were observed at all different rates (see supplementary Fig. S7 online). This sloped voltage profile can be mainly attributed to the decreased crystallite size of TiO<sub>2</sub> and the porous nanostructure of the hybrid material<sup>15</sup>. In the CNT@TiO<sub>2</sub>-C nanocable, the size of TiO<sub>2</sub> particles is below 8 nm and these particles are isolated by carbon layer to constrain the direct connection and growth of primary particles which provides much more surface/interfacial space for lithium storage.

Figure 5c displays the rate capability of the CNT@TiO<sub>2</sub>-C nanocable at different rates from 0.5C to 50C, and the results for the CNT/TiO<sub>2</sub> and the commercial TiO<sub>2</sub> nanoparticle are also included for



**Figure 4** | SEM images of (a,b) CNT/TiO<sub>2</sub> composite prepared by hydrothermal reaction in the absence of glucose and (c,d) TiO<sub>2</sub> nanoparticles prepared by hydrothermal reaction in the absence of glucose and CNT.





**Figure 5 | Electrochemical measurements.** (a) Representative cyclic voltammograms of the CNT@TiO<sub>2</sub>-C nanocable electrode at a scan rate of 0.1 mV s<sup>-1</sup>; (b) The first charge-discharge voltage profiles and (c) The rate capability of the CNT@TiO<sub>2</sub>-C nanocable, CNT/TiO<sub>2</sub> composite and commercial TiO<sub>2</sub> nanoparticle electrodes; (d) Comparison of rate-capability of a variety of TiO<sub>2</sub>-based high-rate electrodes reported recently. TiO<sub>2</sub>-graphene<sup>16</sup>, CNT-TiO<sub>2</sub> nanocrystals<sup>13</sup>, TiO<sub>2</sub>-RuO<sub>2</sub><sup>13</sup>, TiO<sub>2</sub> nanosheets<sup>42</sup>, TiO<sub>2</sub> mesocrystals<sup>43</sup>, SWCNT-TiO<sub>2</sub><sup>10</sup>, TiO<sub>2</sub> nanosphere/graphene<sup>44</sup>.

comparison. The rate comparison between the CNT@TiO<sub>2</sub>-C nanocable and the TiO<sub>2</sub> nanoparticle prepared by similar processes is also provided in supplementary Fig. S8. As expected, the CNT@TiO<sub>2</sub>-C nanocable exhibits superior rate capability compared to the counterparts at the same testing condition, with the charge capacity of 210 mA h g<sup>-1</sup> at 10C, 178 mA h g<sup>-1</sup> at 20C, and 127 mA h g<sup>-1</sup> at 50C. More importantly, a stable capacity of 285 mA h g<sup>-1</sup> can be delivered when the rate was reduced back to 0.5C, suggesting good structural stability of the nanocable and high reversibility even after high rate charge-discharge. It should be noted that the high-rate capability is similar to the best nanostructured or hybrid TiO<sub>2</sub> electrodes reported so far under similar testing conditions as shown in Figure 5d<sup>10,11,13,16,17,38–44</sup>. Such excellent electrochemical performance can be attributed to the following aspects. The nanosized TiO<sub>2</sub> particles reduce Li<sup>+</sup> diffusion distance and increase the surface/interfacial space for lithium storage, which facilitates the ionic and electronic transport and provides additional supercapacitance capacity contribution. Furthermore, the three-dimensional conductive network around each TiO<sub>2</sub> nanoparticle formed by the inner CNT core and the outer carbon layer significantly improves the entire electronic conductivity of the nanocable to facilitate the electrochemical processes, even charge-discharge at high rate. Besides, the mesoporous

structure of the nanocable ensures more particles to be wetted by the liquid electrolyte, thus improving the rate performance.

To evaluate the cyclability at high rate, we cycled the CNT@TiO<sub>2</sub>-C nanocable at high rate of 5C and 50C over 2000 cycles. It can be seen clearly in Fig. 6 that the CNT@TiO<sub>2</sub>-C nanocable demonstrates excellent cycling stability with a charge capacity of 187 mA h g<sup>-1</sup> after 2000 cycles at 5C, keeping a capacity retention of 90%. Even at extremely high rate of 50C, the CNT@TiO<sub>2</sub>-C nanocable still delivers high charge capacity of 122 mA h g<sup>-1</sup> after 2000 cycles with the capacity retention of 87%. This is far superior to the conventional TiO<sub>2</sub> anodes, typically with capacity fading of over 20% after 1000 cycles. Such superior electrochemical performances are very promising to meet the requirements for many long-term high-power applications.

In summary, a new nanostructure, CNT@TiO<sub>2</sub>-C nanocables were produced by a simple and green hydrothermal process. Using glucose as a structure-directing agent and carbon source, there is no need for any treatments for covalent/non-covalent functionalization of CNTs. Glucose was found to play multiple roles in the formation of the nanocable, including improving the interfacial interaction between TiO<sub>2</sub> and CNT to facilitate the TiO<sub>2</sub> nucleation on the surface of CNTs, controlling the growth of TiO<sub>2</sub> nanoparticles, and

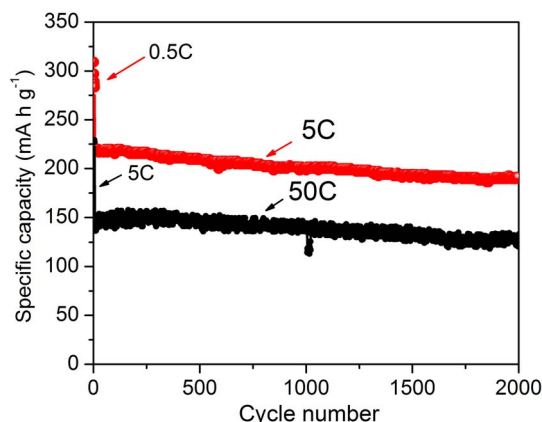


**Figure 6** | Cycling performance of the CNT@TiO<sub>2</sub>-C nanocable electrode at high current rate of 5C and 50C (the first 5 cycles is cycled at low rate).

producing three-dimensional carbon conductive network with the CNT core around the TiO<sub>2</sub> nanoparticles. The synergistic effect of the reduced particle size, high electronic conductivity provided by inner CNT/outer carbon layer, mesoporous structure, and high surface area leads to superior electrochemical performance. It demonstrates excellent high-rate long-term cycling stability with a high charge capacity of 187 mA h g<sup>-1</sup> after 2000 cycles at 5C and 122 mA h g<sup>-1</sup> after 2000 cycles at 50C.

It is worth pointing out that the synthetic methodology used in this study is very simple and green, compared to the previously reported method with more complex synthetic procedures<sup>12,38</sup>, which is promising for many industrial applications. We anticipate that the one-pot synthesis method proposed in this study will provide more choices for addressing the problems of LIBs.

## Methods

**Material and synthesis.** CNT@TiO<sub>2</sub>-C nanocables were synthesized by hydrothermal method and subsequent thermally treatment. Briefly, 1.0 ml titanium isopropoxide (98%, Sigma-Aldrich), 0.2 g glucose (Alfa Aesar), and 30 mg CNT (multiwalled carbon nanotube, Sigma-Aldrich, carbon >90%, trace metal basis) were added in 15 ml alcohol. The solution was further sonicated for 1 h, then transferred into an autoclave, and kept at a temperature of 180°C for 40 h. The resulting black solid products were centrifuged, washed ethanol several times, and then dried at 75°C in a drying oven. Finally, the products were treated in a tubular furnace at 500°C for 3 h under N<sub>2</sub> at a ramping rate of 5°C/min. CNT/TiO<sub>2</sub> composites were synthesized by the same method as described above, except that there was no glucose involved.

**Material characterization.** X-ray diffraction (XRD) patterns were carried out by using a Panalytical diffractometer. The morphologies were characterized by using field emission scanning electron microscopy (FE-SEM, JEOL 7500) and high resolution transmission electron microscopy (HRTEM, 200 kV FEI monochromated F20 UT Tecnai). The thermogravimetric analysis (TGA, Perkin Elmer TGA7) was carried out at a heating rate of 20°C/min from room temperature to 700°C with airflow. Pore size distributions were calculated from the adsorption branch of the N<sub>2</sub> adsorption-desorption isotherm using a Brunauer-Emmett-Teller surface area analyzer (BET, Micromeritics ASAP2020), and a Hall Effect measurement system (HMS-5000). Raman spectra were collected in the backscattering configuration using a micro-Raman spectrometer (Labram, ISA Groupe Horiba).

**Electrochemical measurements.** The TiO<sub>2</sub> electrode was prepared by mixing the prepared active component with acetylene black and polyvinylidene difluoride (PVDF) in a weight ratio of 8 : 1 : 1. The resultant slurry was then uniformly casted on pure Cu foil current collector and dried overnight under vacuum. The counter electrode was lithium foil for a half cell. The C-rate used is based on the anatase theoretical capacity of 168 mA h/g<sup>10,15,16</sup>. The electrolyte used was a solution of 1 M LiPF<sub>6</sub> in ethylene carbonate/dimethyl carbonate (1 : 2). The cells were galvanostatically charged and discharged at different current densities in a range of 1–3.0 V.

1. Zhu, Y. F., Shi, J. J., Zhang, Z. Y., Zhang, C. & Zhang, X. R. Development of a gas sensor utilizing chemiluminescence on nanosized titanium dioxide. *Anal. Chem.* **74**, 120–124 (2002).

2. Carp, O., Huisman, C. L. & Reller, A. Photoinduced reactivity of titanium dioxide. *Prog. Solid. State. Ch.* **32**, 33–177 (2004).
3. Ren, Y. *et al.* Nanoparticulate TiO<sub>2</sub>(B): An Anode for Lithium-Ion Batteries. *Angew. Chem. Int. Ed.* **51**, 5 (2012).
4. Ji, L., Lin, Z., Alcoutlabi, M. & Zhang, X. Recent developments in nanostructured anode materials for rechargeable lithium-ion batteries. *Energy. Environ. Sci.* **4**, 2682 (2011).
5. Deng, D., Kim, M. G., Lee, J. Y. & Cho, J. Green energy storage materials: Nanostructured TiO<sub>2</sub> and Sn-based anodes for lithium-ion batteries. *Energy. Environ. Sci.* **2**, 818 (2009).
6. Liu, R., Duay, J. & Lee, S. B. Heterogeneous nanostructured electrode materials for electrochemical energy storage. *Chem. Commun.* **47**, 1384 (2011).
7. Sudant, G., Baudrin, E., Larcher, D. & Tarascon, J. M. Electrochemical lithium reactivity with nanotextured anatase-type TiO<sub>2</sub>. *J. Mater. Chem.* **15**, 1263–1269 (2005).
8. Shin, J.-Y., Samuelis, D. & Maier, J. Sustained Lithium-Storage Performance of Hierarchical, Nanoporous Anatase TiO<sub>2</sub> at High Rates: Emphasis on Interfacial Storage Phenomena. *Adv. Funct. Mater.* **21**, 3464–3472 (2011).
9. Wagemaker, M., Borghols, W. J. H. & Mulder, F. M. Large impact of particle size on insertion reactions. A case for anatase LiTiO<sub>2</sub>. *J. Am. Chem. Soc.* **129**, 4323–4327 (2007).
10. Moriguchi, I. *et al.* A Mesoporous Nanocomposite of TiO<sub>2</sub> and Carbon Nanotubes as a High-Rate Li-Intercalation Electrode Material. *Adv. Mater.* **18**, 69–73 (2006).
11. Saravanan, K., Ananthanarayanan, K. & Balaya, P. Mesoporous TiO<sub>2</sub> with high packing density for superior lithium storage. *Energy. Environ. Sci.* **3**, 939 (2010).
12. Liu, H. *et al.* Mesoporous TiO<sub>2</sub>-B Microspheres with Superior Rate Performance for Lithium Ion Batteries. *Adv. Mater.* **23**, 3450–3454 (2011).
13. Guo, Y. G., Hu, Y. S., Sigle, W. & Maier, J. Superior Electrode Performance of Nanostructured Mesoporous TiO<sub>2</sub> (Anatase) through Efficient Hierarchical Mixed Conducting Networks. *Adv. Mater.* **19**, 2087–2091 (2007).
14. Cao, F. F. *et al.* Symbiotic Coaxial Nanocables: Facile Synthesis and an Efficient and Elegant Morphological Solution to the Lithium Storage Problem. *Chem. Mater.* **22**, 1908–1914 (2010).
15. Park, K.-S. *et al.* Long-term, high-rate lithium storage capabilities of TiO<sub>2</sub> nanostructured electrodes using 3D self-supported indium tin oxide conducting nanowire arrays. *Energy. Environ. Sci.* **4**, 1796 (2011).
16. Wang, D. H. *et al.* Self-Assembled TiO<sub>2</sub>(2)-Graphene Hybrid Nanostructures for Enhanced Li-Ion Insertion. *ACS. Nano.* **3**, 907–914 (2009).
17. Chen, J. S., Wang, Z., Dong, X. C., Chen, P. & Lou, X. W. Graphene-wrapped TiO<sub>2</sub> hollow structures with enhanced lithium storage capabilities. *Nanoscale* **3**, 2158 (2011).
18. Park, S.-J., Kim, H., Kim, Y.-J. & Lee, H. Preparation of carbon-coated TiO<sub>2</sub> nanostructures for lithium-ion batteries. *Electrochim. Acta* **56**, 5355–5362 (2011).
19. Park, S.-J., Kim, Y.-J. & Lee, H. Synthesis of carbon-coated TiO<sub>2</sub> nanotubes for high-power lithium-ion batteries. *J. Power. Sources* **196**, 5133–5137 (2011).
20. Cui, L. F., Hu, L. B., Choi, J. W. & Cui, Y. Light-Weight Free-Standing Carbon Nanotube-Silicon Films for Anodes of Lithium Ion Batteries. *ACS Nano* **4**, 3671–3678 (2010).
21. Ding, S. J., Chen, J. S. & Lou, X. W. One-Dimensional Hierarchical Structures Composed of Novel Metal Oxide Nanosheets on a Carbon Nanotube Backbone and Their Lithium-Storage Properties. *Adv. Funct. Mater.* **21**, 4120–4125 (2011).
22. Zhang, H.-X. *et al.* Cross-Stacked Carbon Nanotube Sheets Uniformly Loaded with SnO<sub>2</sub> Nanoparticles: A Novel Binder-Free and High-Capacity Anode Material for Lithium-Ion Batteries. *Adv. Mater.* **21**, 2299–2304 (2009).
23. Hu, L. B., Wu, H., La Mantia, F., Yang, Y. A. & Cui, Y. Thin, Flexible Secondary Li-Ion Paper Batteries. *ACS Nano* **4**, 5843–5848 (2010).
24. Eder, D. & Windle, A. H. Carbon-Inorganic Hybrid Materials: The Carbon-Nanotube/TiO<sub>2</sub> Interface. *Adv. Mater.* **20**, 1787–1793 (2008).
25. Eder, D. & Windle, A. H. Morphology control of CNT-TiO<sub>2</sub> hybrid materials and rutile nanotubes. *J. Mater. Chem.* **18**, 2036–2043 (2008).
26. Eder, D. Carbon Nanotube-Inorganic Hybrids. *Chem. Rev.* **110**, 1348–1385 (2010).
27. Bian, Z. F. *et al.* Solvothermal synthesis of well-defined TiO<sub>2</sub> mesoporous nanotubes with enhanced photocatalytic activity. *Chem. Commun.* **46**, 8451–8453 (2010).
28. Cao, F.-F., Guo, Y.-G. & Wan, L.-J. Better lithium-ion batteries with nanocable-like electrode materials. *Energy. Environ. Sci.* **4**, 1634 (2011).
29. Cooke, D. J., Eder, D. & Elliott, J. A. Role of Benzyl Alcohol in Controlling the Growth of TiO<sub>2</sub> on Carbon Nanotubes. *J. Phys. Chem. C* **114**, 2462–2470 (2010).
30. Lou, X. W., Chen, J. S., Chen, P. & Archer, L. A. One-Pot Synthesis of Carbon-Coated SnO<sub>2</sub>Nanocolloids with Improved Reversible Lithium Storage Properties. *Chem. Mater.* **21**, 2868–2874 (2009).
31. Sun, X. M. & Li, Y. D. Colloidal carbon spheres and their core/shell structures with noble-metal nanoparticles. *Angew. Chem. Int. Edit.* **43**, 597–601 (2004).
32. Luo, L. B., Yu, S. H., Qian, H. S. & Gong, J. Y. Large scale synthesis of uniform silver@carbon rich composite (carbon and cross-linked PVA) sub-microcables by a facile green chemistry carbonization approach. *Chem. Commun.* 793–795 (2006).



33. Sakaki, T., Shibata, M., Miki, T., Hirose, H. & Hayashi, N. Reaction model of cellulose decomposition in near-critical water and fermentation of products. *Bioresource Technol.* **58**, 197–202 (1996).
34. Qiao, H., Zheng, Z., Zhang, L. & Xiao, L. SnO<sub>2</sub>@C core-shell spheres: synthesis, characterization, and performance in reversible Li-ion storage. *J. Mater. Sci.* **43**, 2778–2784 (2008).
35. Sun, X. M., Liu, J. F. & Li, Y. D. Use of carbonaceous polysaccharide microspheres as templates for fabricating metal oxide hollow spheres. *Chem-Eur. J.* **12**, 2039–2047 (2006).
36. Kavan, L., Gratzel, M., Rathousky, J. & Zukal, A. Nanocrystalline TiO<sub>2</sub> (anatase) electrodes: Surface morphology, adsorption, and electrochemical properties. *J. Electrochem. Soc.* **143**, 394–400 (1996).
37. Wang, J., Polleux, J., Lim, J. & Dunn, B. Pseudocapacitive contributions to electrochemical energy storage in TiO<sub>2</sub> (anatase) nanoparticles. *J. Phys. Chem C.* **111**, 14925–14931 (2007).
38. Liu, J. H., Chen, J. S., Wei, X. F., Lou, X. W. & Liu, X. W. Sandwich-Like, Stacked Ultrathin Titanate Nanosheets for Ultrafast Lithium Storage. *Adv. Mater.* **23**, 998–1002 (2011).
39. Yang, S. B., Feng, X. L. & Mullen, K. Sandwich-Like, Graphene-Based Titania Nanosheets with High Surface Area for Fast Lithium Storage. *Adv. Mater.* **23**, 3575–3579 (2011).
40. Zhu, P. N. *et al.* Long term cycling studies of electrospun TiO<sub>2</sub> nanostructures and their composites with MWCNTs for rechargeable Li-ion batteries. *Rsc Adv.* **2**, 531–537 (2012).
41. Chen, Z. *et al.* High-Performance Energy-Storage Architectures from Carbon Nanotubes and Nanocrystal Building Blocks. *Adv. Mater.* **24**, 2030–2036 (2012).
42. Liu, J., Chen, J. S., Wei, X., Lou, X. W. & Liu, X.-W. Sandwich-Like, Stacked Ultrathin Titanate Nanosheets for Ultrafast Lithium Storage. *Adv. Mater.* **23**, 998–1002 (2011).
43. Ye, J. *et al.* Nanoporous Anatase TiO<sub>2</sub> Mesocrystals: Additive-Free Synthesis, Remarkable Crystalline-Phase Stability, and Improved Lithium Insertion Behavior. *J. Am. Chem. Soc.* **133**, 933–940 (2011).
44. Li, N. *et al.* Battery Performance and Photocatalytic Activity of Mesoporous Anatase TiO<sub>2</sub> Nanospheres/Graphene Composites by Template-Free Self-Assembly. *Adv. Funct. Mater.* **21**, 1717–1722 (2011).

## Acknowledgments

This work was supported by the Startup Foundation of China Academy of Engineering Physics, Institute of Chemical Materials (KJCX201301 and KJCX201306) and National High-tech Research and Development Program (863 Program: No.2013AA050905). The authors acknowledge support of the National Center for Electron Microscopy, Lawrence Berkeley Lab, which is supported by the U.S. Department of Energy under Contract # DE-AC02-05CH11231.

## Author contributions

J.L.C. and B.W. designed and carried out research, analyzed data and wrote the paper. H.L.X. conducted the TEM measurements. X.D.L., G.C.Y. and F.D.N. also contributed extensively to the work presented in this paper. All authors reviewed the manuscript.

## Additional information

**Supplementary information** accompanies this paper at <http://www.nature.com/scientificreports>

**Competing financial interests:** The authors declare no competing financial interests.

**How to cite this article:** Wang, B. *et al.* Mesoporous CNT@TiO<sub>2</sub>-C Nanocable with Extremely Durable High Rate Capability for Lithium-Ion Battery Anodes. *Sci. Rep.* **4**, 3729; DOI:10.1038/srep03729 (2014).



This work is licensed under a Creative Commons Attribution-NonCommercial-NoDerivs 3.0 Unported license. To view a copy of this license, visit <http://creativecommons.org/licenses/by-nc-nd/3.0>